Self-assembly and Photo-patterning in Polymer-fullerene Nanocomposite Thin Films

ARTICLE · MARCH 2013

READS
15

5 AUTHORS, INCLUDING:

Him Cheng Wong
Singapore University of Technology and De…
19 PUBLICATIONS **202** CITATIONS
SEE PROFILE

Anthony M Higgins
Swansea University
31 PUBLICATIONS **829** CITATIONS
SEE PROFILE

J. F. Douglas
National Institute of Standards and Techno…
425 PUBLICATIONS **14,587** CITATIONS
SEE PROFILE

João T Cabral
Imperial College London
85 PUBLICATIONS **1,217** CITATIONS
SEE PROFILE

Patterning Polymer–Fullerene Nanocomposite Thin Films with Light

*Him Cheng Wong, Anthony M. Higgins, Andrew R. Wildes, Jack F. Douglas, and João T. Cabral**

Trace amounts of C_{60} fullerene impart stability to thin polymer films against dewetting by the combined effects of pinning the contact lines of dewetting holes and by effectively altering the polymer-substrate interaction.[1,2] Polymer nanocomposite thin films of higher molecular mass (M_w) yield well-defined morphologies from uniform to spinodal-like, via spontaneous polymer–fullerene phase separation and crystallization.[3,4] In this paper, we report that UV-visible, and even background, light exposure, is a strong contributing factor to (i) dewetting suppression and (ii) nanoparticle association in polymer-C_{60} thin films. We find a coupling of fullerene photo-sensitivity and both self-assembly processes which results in controlled pattern formation, and we illustrate the effect with a model polystyrene–fullerene (PS–C_{60}) circuit pattern. This approach opens new opportunities in soft matter lithography via the directed assembly of polymer nanocomposites and underscores their photoactive nature, an effect of great interest to material performance and stability of organic photovoltaics (OPV) and aerospace materials under long-term radiation exposure.

The physical mechanism responsible for dewetting suppression in nanoparticle-filled polymer thin films has been associated with an entropically driven substrate segregation[5] of the nanoadditives, including fullerenes and derivatives, dendrimers, and many other nanoscale filler particles.[1,2,6,7] **Figure 1** depicts the striking fullerene-induced dewetting suppression of low M_w PS(2k)-C_{60} thin films cast on a silicon substrate (surface energy $\sigma = 69 \pm 1$ mN·m^{-1}, referred to as surface 'σ'). Since its discovery, both kinetic effects associated with contact line pinning of growing holes and changes of the polymer-surface interaction have been suggested as explanations[1,6] of this technologically important phenomenon. Here, we demonstrate that there is an additional highly relevant factor that is responsible for the stability of polymer–fullerene films. In particular, we show a clear correlation between the stability-dewetting transition of low M_w polymer films and exposure to *light*. If the polymer film is kept in the dark, complete film stabilization is inaccessible and, instead, film dewetting is retarded with increasing C_{60} concentration, as seen on the left side of each panel of Figure 1 ("dark"). Furthermore, we unequivocally show that the stability of low M_w PS(2k) nanocomposite thin films is greatly enhanced when thermal annealing is *preceded* by a light exposure step, yielding complete stability beyond 2% C_{60} loading (indicated as% mass fraction throughout the paper). The left panel of Figure 1 reports the control experiment, confirming that neat PS dewets upon annealing at 180 °C regardless of light exposure and the observed light induced dewetting suppression effect is indeed caused by the fullerenes in the polymer thin film. Both UV and visible light are remarkably effective in dewetting suppression and it is particularly surprising to us that, even low intensity ambient room light suffices, albeit requiring longer times to achieve the same effect. The results shown in Figure 1, corroborated by atomic force microscopy (AFM), correspond to a low intensity UV (365 nm, 0.2 mW/cm^2, 3 h) exposure according to the schematic on the bottom left panel of Figure 1, followed by step annealing at 100, 140, and 180 °C for 30 min each; similar results are obtained after ≈ 24 h of ambient light exposure. The light driven dewetting suppression effect evidently depends on the fullerene loading in the film, and we find a threshold for complete film stabilization of ≈ 2%, which agrees well with the PS-C_{60} miscibility threshold (1-2%) reported earlier.[4,8,9]

The reported light induced dewetting suppression effect is robust to a wide variation of substrate properties, illustrated by three silicon substrate treatments ('σ', 'σ-', 'σ+') shown in **Figure 2**a–c for PS(2k) films with 5% C_{60} loading ($h \approx 35 \pm 1$ nm). Of course, the stability of low M_w nanocomposite films also depends strongly on substrate surface energy (viz., $\sigma = 69 \pm 1$, $\sigma- = 41 \pm 1$ and $\sigma+ = 72.5 \pm 0.5$ mNm^{-1}). On substrates σ+, nanocomposite films containing about 5% C_{60} do not dewet after annealing for many hours. Instead, we observe a lateral association of the fullerenes (Figure 2a) into circular agglomerates that eventually crystallize.[4] The magnified view of the small inset images (labelled * and **) are depicted in Figure 2d. The characteristic lengthscales and coordination of this (spinodal-like) correlated nucleation morphology[3] scales with film thickness and pins at long annealing times (> 3 h to 6 h), consistent with 2D phase separation of binary mixtures.[10] Similar observations are found for nanocomposite films of various M_w, as shown in Figure 2e and 2f for 110-nm PS(2k) and PS(270k) films with 5% C_{60} loading. With increasing polymer M_w, the

Dr. H. C. Wong, Dr. J. T. Cabral
Department of Chemical Engineering and
Centre for Plastic Electronics
Imperial College
London, London SW7 2AZ, UK
E-mail: j.cabral@imperial.ac.uk
Dr. A. M. Higgins
Multidisciplinary Nanotechnology Centre
College of Engineering
Swansea University
Swansea SA2 8PP, UK
Dr. A. R. Wildes
Institut Laue-Langevin, B.P. 156, 38042 Grenoble, France
Dr. J. F. Douglas
National Institute of Standards and Technology, Gaithersburg, USA

DOI: 10.1002/adma.201203541

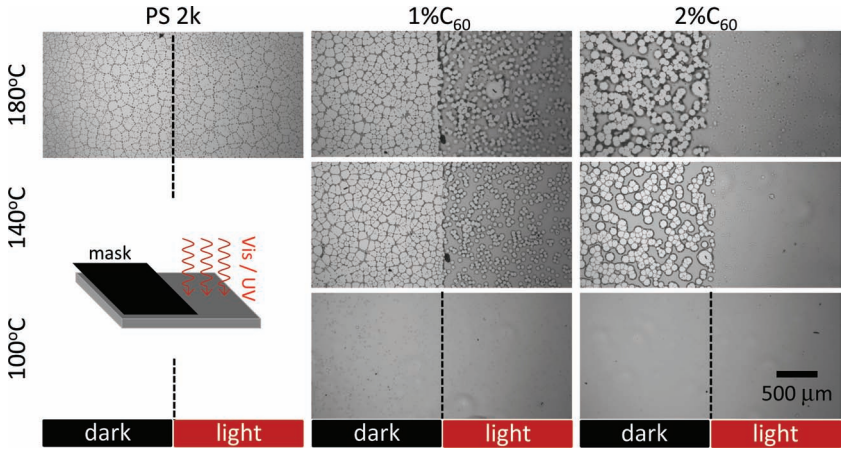

Figure 1. Light-induced film stabilization. Schematic of partial light exposure setup and optical microscopy images of low M_w PS(2k) and nanocomposite thin films ($h = 35 \pm 3$ nm) supported on silicon substrates (σ) and exposed to UV light for 3 h before annealing at 100, 140, and 180 °C for 30 min. Apart from neat PS films that dewet regardless of light exposure, film stability is gradually improved with increasing C_{60} loading, and critically on the illuminated side.

dominant structural scale λ^* decreases (for the same annealing time), because of the higher film viscosity.[4] PS(270k)-5% C_{60} nanocomposite films have been studied previously,[3] and $\lambda^*(t=0)$ has been found to scale linearly with film thickness, while the resulting coarsening kinetics follow $\lambda^* \sim t^{\alpha}$, before structural pinning, with α ranging from 1/3 in 'thick' films (viz. h >150 nm) to $\alpha \rightarrow 0$ for ultra-thin films (h < 20 nm). Hence, for non-dewetted nanocomposite films, visible white light exposure results in the suppression of C_{60} agglomeration, drastically reducing λ^* and the average surface topography amplitude $<\delta h>$. The power law for coarsening kinetics for a given film thickness remains unchanged with light exposure, but the characteristic lengthscales of the morphology decrease considerably, as does the onset time and lenght scale of structural pinning.

Higher M_w nanocomposite films are comparatively less responsive to surface energy, as dewetting kinetics are considerably slower, even on rather unfavorable substrates (σ-). As a result, film dewetting occurs in a much longer timescale than fullerene association and thus always results in spinodal-like correlated nucleation. As polymer M_w decreases, substrate surface energy becomes increasingly significant. For substrates with slightly lower wettability (σ), a film of 35 nm of PS(2k)-5% C_{60} dewets upon thermal annealing, as seen on the left side of Figure 2b. Again, if thermal annealing is preceded by UV light exposure for 6 h, the film remains stable against dewetting as shown on the right side of Figure 2b. In the "dark", we observe an unusually small and irregular dewetting pattern at relatively high fullerene loading (5%), resulting from the simultaneous dewetting and fullerene association. Finally, for a substrate with the most adverse wetting property in this study (σ-), the same fullerene nanocomposite thin film dewets almost instantly (<2 s) upon annealing at 180 °C on the side unexposed to light, resulting in the usual Voronoi tessellation dewetting pattern,[11] as seen on the left side of Figure 2c. In contrast, complete film dewetting inhibition is observed on the same film, when exposed to the same dose of UV radiation prior to thermal annealing, as shown on the right side of Figure 2c. The combined action of fullerenes and light exposure can dramatically stabilize the film against dewetting. There are clearly more factors involved in the dewetting suppression process for this system than just C_{60} segregation to the substrate interface and the resulting influence on the rate of dewetting through contact line pinning and changes of the thermodynamic interaction at the boundary.

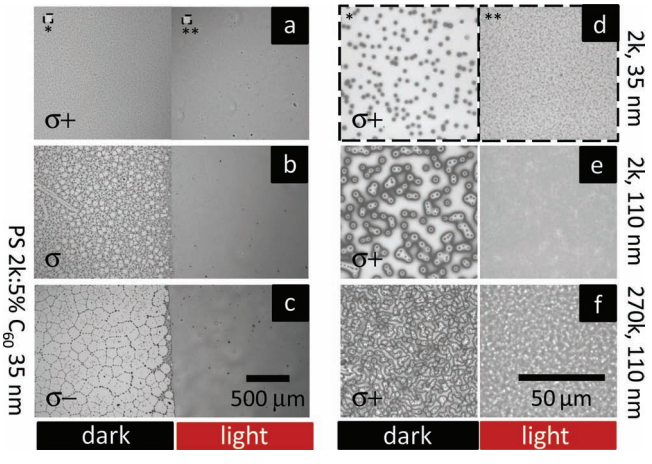

Figure 2. Effect of substrate wettability on film stability and fullerene association. (a-c): 35 nm PS(2k) films with 5% C_{60} on substrates with surface energy σ+, σ and σ- (see text). Inset images (labeled * and **) are magnified in panel (d). All films (d,e,f) were cast on substrates σ+; (d) PS(2k)-5% C_{60} $h \approx 35$ nm; (e) PS(2k)-5% C_{60} $h \approx 110$ nm; (f) PS(270k)-5% C_{60} $h \approx 110$ nm. Films were exposed to light for 6 h, using the setup depicted in Figure 1, and subsequently annealed at 180 °C for 30 min immediately after light exposure.

In order to elucidate the origin of this striking light-induced thin film stabilization and light-controlled fullerene association effect, we evaluate the fullerene depth-composition profile in our as-cast films, prior and after light exposure, using neutron reflectivity (NR). **Figure 3**a shows the NR data for as-cast films of neat PS(270k), PS(270k)-5% C_{60} and PS(2k)-5% C_{60}. The solid lines are best fits to the data, using a two-layer model consisting of a 'bulk' layer with homogeneously distributed C_{60} fullerenes and a thin (≈ 1 nm) native oxide layer. The corresponding scattering length density (ρ_b) profiles, in Figure 3b, shows that the 'bulk' film is markedly different in the neat and 5% nanocomposite films, confirming that NR can accurately quantify C_{60} loading at this level.

Qualitatively, the shallower first minimum and deeper remaining minima of the neat PS NR data compared to the PS-5% C_{60} sets (see inset of Figure 3a) is indicative of a sample with lower ρ_b in the "bulk" film, as expected from the neat PS(270k) film. From the ρ_b profiles in Figure 3b, we also conclude that the fullerenes are uniformly dispersed orthogonally to film surface with no evidence of an extra C_{60}-rich layer at the substrate (although non-uniform distribution is certainly

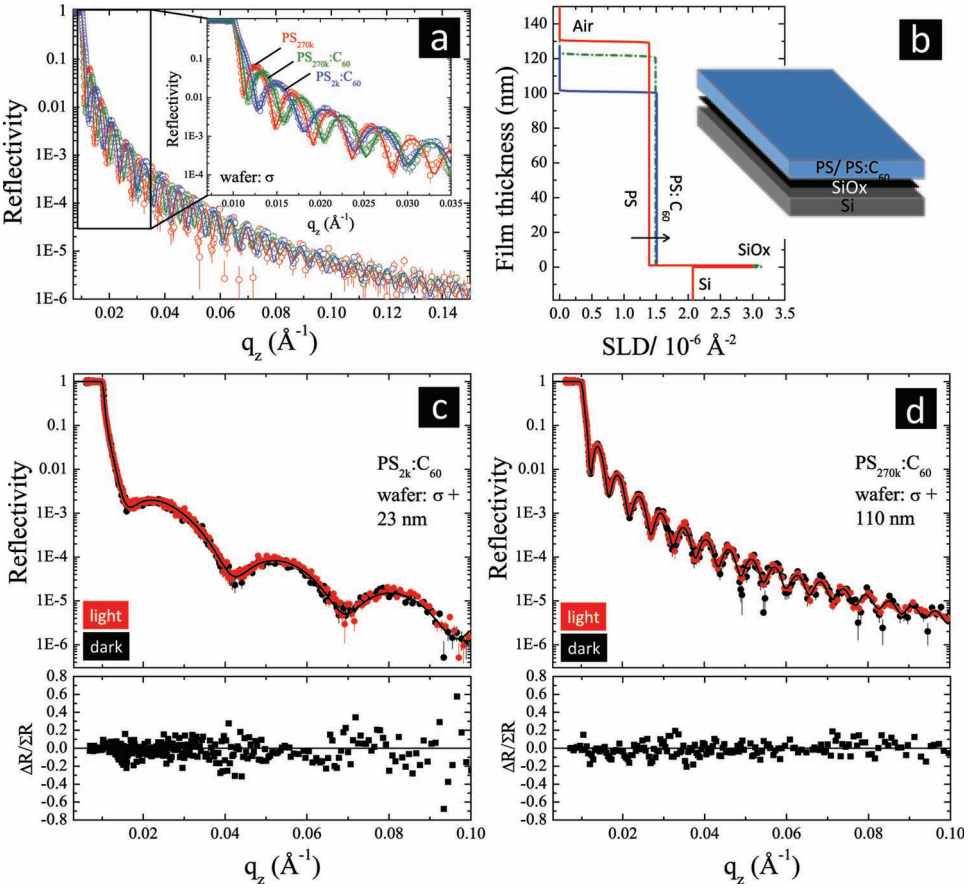

Figure 3. Effect of light illumination on C_{60} depth profile. a,b) Neutron reflectivity and scattering length density profiles for as-cast films: (red) 129 nm-neat PS(270k); (green) 121nm-PS(270k)-5% C_{60}; (blue) 100 nm-PS(2k)-5% C_{60} (all substrate σ). c) 23 nm-PS(2k)-5% C_{60} (substrate σ+). d) 110 nm-PS(270k)-5% C_{60} (substrate σ+). For c,d) black profiles denotes as-cast films while red profiles represent films after exposure to visible white light (6 h). The difference between the spectra before and after light exposure are shown below the respective reflectivity data. Solid lines are best fit to the data based on the model explained in text. Fitting parameters are compiled in Supporting Information Table 1.

possible for certain thermal and solvent treatments[1,2]). Moreover, this uniformity of dispersion seems to apply regardless of film thickness, substrate type and polymer matrices M_w that we have studied.

Figure 3c and d shows NR profiles of as-cast nanocomposite films before and after exposure to light. Figure 3c compares $a \approx$ 20 nm PS(2k)-5% C_{60} film cast on substrate σ+, before (black) and after (red) visible light exposure for 6 h. Possible effects of matrix M_w or film thickness are considered with a slightly thicker ≈ 110 nm PS(270k)-5% C_{60} film, as shown in Figure 3d. The differences between the NR spectra prior and post light exposure are shown below the respective data sets and minimal changes are found, within experimental uncertainty. (Comprehensive NR data sets for various film thickness, M_w and substrate energy in Supporting Information Figure S1). We conclude that illumination does not induce fullerene spatial rearrangement in films of any parameters studied above (cf. Supporting Information Figure S2), but the resulting annealed film morphology and stability changes drastically in comparison to the unexposed counterpart (see Figure 1 and 2).

Hitherto, the formation of a nanoparticle layer at the substrate interface has been linked to dewetting suppression in low M_w thin films.[1,2,6,7] However, in our system, C_{60} fullerenes remain homogeneously distributed in the "bulk" layer according to our NR results, so a different mechanism must become active upon illumination. In the absence of light exposure, dewetting suppression of PS-C_{60} films during annealing can happen if fullerene substrate diffusion kinetics is faster than film dewetting kinetics during annealing, thus forming an enriched surface layer. Additional thermal and solvent annealing treatment prior to thermal annealing may thus play a key role.[1,2] Indeed, the diffusion of nanoadditives in polymer thin films has been shown to be faster[12] than the Stokes-Einstein prediction and to be highly anisotropic,[13] i.e., occurring considerably faster on the plane of the film than orthogonally, due to significant lubrication forces in a 2D confined geometry. Under these conditions, the dewetting suppression studied in previous work,[1,2,6,7] which considered low M_w polymers, still applies. In this paper, we show that exposure to light results in film stabilization against dewetting even for films with lower C_{60} loading ($\ll$ 5%), i.e., *without* a C_{60}-enriched surface and on low surface energy substrates (σ-). The extent of the light induced film stabilization effect depends on the substrate surface energy, C_{60} loading and film thickness, the latter two governing the total amount of C_{60}

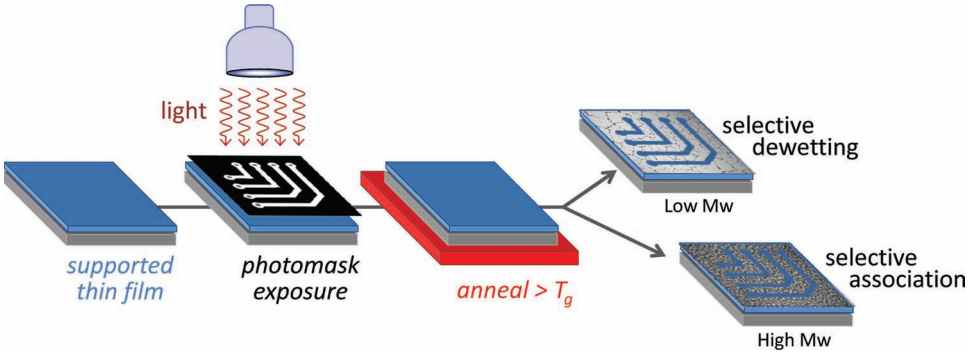

Figure 4. Patterning schematic. Polymer–fullerene films are prepared by spin coating and then illuminated through a photomask, followed by thermal annealing above T_g; in low M_w films, dark areas dewet, while illuminated areas remain (meta)stable. High M_w films (or supported by high σ surfaces) exhibit fullerene association on a lengthscale defined by the phase separation process and dependent on illumination dose (intensity x time).

in the thin film. The dewetting-stable transition of the illuminated PS(2k)-C_{60} nanocomposite films ($T = 140$ °C) ranges from ≈ 1% C_{60} loading (substrate σ+; $h \approx 35$ nm) to ≈2% (substrate σ; $h \approx 35$ nm) to ≈ 3% (substrate σ+; $h \approx 20$ nm). Establishing this phenomenon is the primary result of our paper.

The underpinning physical mechanism of this photostabilization effect is rationalized in terms of well-known photo-chemical transformations of fullerenes (and derivatives), namely photo-oxidation and photo-polymerization,[14] which can occur in the pure state[14–16] and in solution.[17,18] Indeed, illuminated fullerenes can generate highly reactive radical species that can chemically react with their surrounding environment, causing for example oxidative damage to lipid membranes of living systems.[18]

C_{60} photo-oxidation[19] occurs when fullerenes are simultaneously exposed to oxygen and UV-visible light, which enhances O_2 diffusion into interstitial voids of the fcc fullerene lattice by more than one order of magnitude, eventually forming oxidized fullerenes $C_{60}(O_2)_x$, by replacing C=C bonds of the C_{60} cage with two adjacent carbonyl C=O groups. C_{60} photo-polymerization,[20] on the other hand, results in intermolecular C-C bonds between C_{60}, but only occurs when illuminated in vacuum or inert atmosphere, as O_2 inhibits the polymerization reaction. In order to ascertain which mechanism is active in our system, controlled illumination experiments in ambient and vacuum conditions were carried out (cf. Supporting Information Figure S3), unequivocally demonstrating that photo-oxidation is responsible for the observed stabilization and controlled association effects. Simultaneous illumination and air (oxygen) exposure causes fullerene photo-activation and subsequently the formation of a PS-$C_{60}(O_2)_x$ "network".[21] This likely imparts greater film structural integrity which probably contributes to the dewetting suppression through gelation of the film. It is also possible that this 'cross-linking' effect stabilizes the fractal fullerene clusters near the substrate that form in lower molecular mass polymer films where the viscosity is lower. For instance, photo-induced cross-linking of PS with bis-benzophenone[22] is also effective at dewetting suppression.

Selective dissolution and AFM provide valuable insight into the nature of the polymer-C_{60} network photo-transformation. Following illumination through a photomask of a PS-C_{60} thin film, prior to thermal annealing, exposure to tetrahydrofuran (THF) – a selective solvent for PS, but not C_{60} – reveals the removal of most material in masked areas and, in contrast, a layer of scattered material is attached to the substrate in the illuminated area. Following illumination and thermal annealing, selective dissolution indicates that exposed film areas exhibit dense and uniformly-distributed small clusters at the solid interface, in contrast with micron-sized C_{60} clusters scattered in dark areas (cf. Supporting Information Figure S4). These results are robust to changes of polystyrene mass M_w (2–270 kg/mol), provided that films do not dewet, as well as other polymer matrices (including acrylates) and fullerene derivatives including phenyl-C61-butyric acid methyl ester (PCBM). In short, illumination in the presence of air (or oxygen) photo-oxidizes fullerenes which, above a threshold loading, form a network with the polymer preventing dewetting upon thermal annealing and controlling fullerene nucleation.

We next show how modulating light exposure through a photomask can spatially control pattern formation in PS-C_{60} thin films. Substrate chemical modification provides a useful means to particle organization processes in polymer films and mixtures, and this methodology has proven very powerful for creating well defined surface patterns.[23] Recent patterning approaches have exploited the characteristic dimensions of phase separating polymer blends on substrates with pre-patterned surface energy variations. There are many other self-organization processes that can be manipulated to facilitate surface patterning such as film dewetting on topological features created by simply substrate rubbing[24] and self-assembled monolayer strips,[25] or electrostatically driven thin film surface instabilities[26] with a topographically patterned top plate in a sandwich-like setup.

To implement the principles for patterning of polymer nanocomposite films with light, we exploit the propensity of the C_{60} fullerenes in the nanocomposite thin film to photo-oxidize and react with the film matrix when exposed to light. We simply employ a photomask to spatially modulate this process and a heating stage to trigger pattern formation, as shown schematically in **Figure 4**. Depending on various combinations of experimental parameters (specifically polymer M_w, substrate wettability, film thickness, fullerene loading and light intensity),

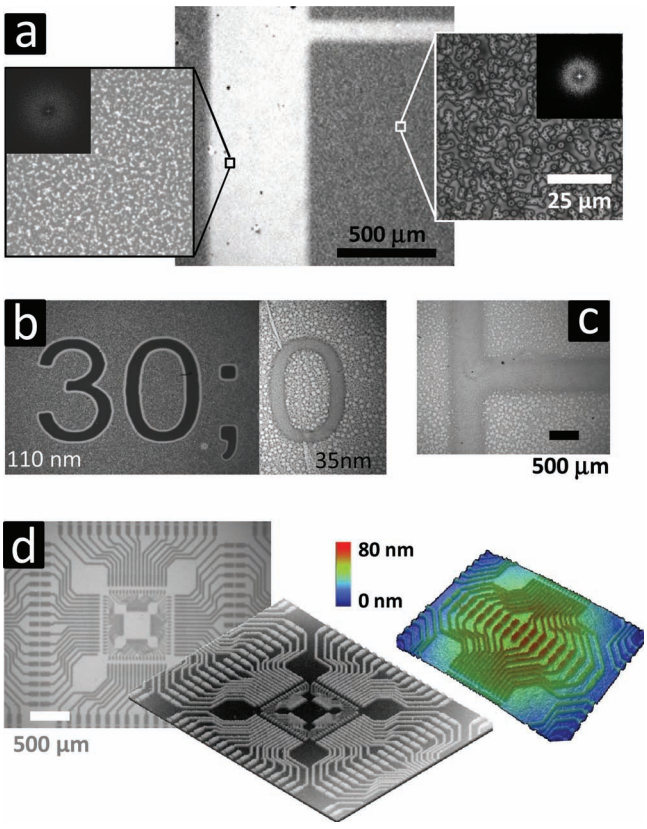

Figure 5. Patterning with light. a) Optical microscopy images of a T-junction channel patterned on a 110nm-PS(270k)-5% C_{60} (substrate σ+). Magnified images show the spinodal-like correlated nucleation morphologies at specific regions of the film. Insets show the fast Fourier transforms (FFT) of the respective lateral morphologies. b) Patterning on PS(2k)-5% C_{60}, h = 110 nm and 35 nm (substrate σ), c. Patterning with film dewetting on 35 nm thick PS(2k)-5% C_{60} (substrate σ). Panels b) and c) share the same scale bar. d) Circuit patterning on same sample type and conditions as in a, yielding a circuit prototype device. Vertical topography of the pattern can be viewed from the 3D optical microscopy images (middle) and optical profilometry scans (right bottom). Samples in a and d were exposed with UV light (6 h) while samples in b and c were exposed with visible white light (6 h). All samples were immediately annealed at 180 °C for 30 min.

the thermally induced fullerene association behavior or thin film dewetting of selected film area can be directed at specific regions of the film, following the photomask pattern. Coupling spatially varying light exposure to self-assembly (film dewetting or C_{60} association) provides a combination of top-down and bottom-up processes reminiscent of block-copolymer ordering assisted by templating substrates.[27] In this way, we achieve a simple and economical method of pattern transfer.

Examples of the patterned features are shown in **Figure 5**. Optical microscopy images in Figure 5a show a T-junction pattern on a 110 nm-PS(270k)-5% C_{60} cast on substrate type σ+. Magnified images show the correlated 'spinodal clustering' morphology, emphasized in our previous work,[3,4] and the structure connectivity at specific regions of the film with and without illumination. The fast Fourier transforms (FFT) of the respective lateral morphologies are depicted in the insets. The UV exposed film area has considerably smaller λ^* and surface undulation amplitude $<\delta h>$. Using the same methodology, a reference number '30;' was patterned on a 110-nm-PS(2k)-5% film cast on substrate σ, as shown in Figure 5b. For this thickness h (125 nm) and M_w (2k), the unexposed film area exhibits a spinodal-like morphology with larger λ^* and $<\delta h>$ in comparison to the exposed area '30;', illustrating the lengthscale tuneability by simply changing M_w. In contrast, if we cross over to a lower film thickness regime, the nanocomposite film dewets on substrate with intermediate wettability (substrate σ), as demonstrated on Figure 5c and the right side of Figure 5b. In this case, the illuminated film area of interest (T-junction strip and the number '0') can remain stable while the surrounding unexposed area dewets upon annealing.

Of course, more elaborate film patterns of technological interest can be replicated onto our nanocomposite films, using appropriate photomasks. As a proof of principle, a circuit pattern has been replicated onto a 110-nm-PS(270k)-5% C_{60} film, as shown in Figure 5d. The vertical topography of the circuit pattern is resolved by microscopy and optical profilometry. Ongoing work involves the optimization of patterning parameters and mapping of conductivity-morphology characteristics at nanoscale resolution using conductive AFM to fabricate functional devices, including OPVs and sensors. Other applications could include patterning scaffolds for tissue engineering and cell growth, where controlled topography and surface properties are key. Our main point here is that there seems to be no difficulty in creating complex patterns of technological interest using our method, although resolution limits remain to be explored, as partly set by the self-organization processes. Further, the *memory*-like effect imprinted by illumination permits a triggered, on-demand, self-assembly by simply heating above the polymer's glass transition. In the field of OPVs, a major challenge remains the prolonging of device lifetime,[28] with acceptable performance and stability. In particular, illumination and (cyclic) thermal and environmental/oxygen exposure largely govern OPV ageing. Detailed mechanistic insight into performance changes with processing, both positive and negative, remains limited. Recent work[29] indicates significant improvements in the power conversion efficiency (1.46% to 4.1%) and stability in 50:50 poly(3-hexylthiophene) (P3HT):PCBM organic solar cells, subjected to post processing illumination prior to testing. Our current findings are therefore significant to morphological control (including tuning dominant lengthscale) and film stability of a range of fullerene-based composites, including in OPVs.

In summary, we demonstrate that the coupling of self-assembly in polymer nanocomposites and photo-transformation provides an extremely promising route for patterning the stability (wetting/dewetting), morphology and characteristic dimensions in thin film composites. Both UV and visible light, even in *ambient conditions*, are effective in suppressing dewetting (or tuning correlated nucleation lengthscales) upon thermal annealing, an effect overlooked in previous work. Our results hold for various polymer matrices (e.g., styrenic and acrylate) and fullerene derivatives (e.g., C_{60} and PCBM) investigated. Photogeneration of reactive species is, in fact, a common phenomenon for other nanoparticles, such as cadmium selenide quantum dots, carbon nanotubes and sheets.[30]

Experimental Section

Thin PS-C_{60} nanocomposite films were prepared by spin coating from dilute PS-C_{60}-toluene solutions. All concentrations (1, 2 and 5%) are indicated in terms of% mass fraction C_{60}. PS M_w = 2.75 kg/mol (M_w/M_n = 1.1, PS(2k)) and 270 kg/mol (M_w/M_n = 2.4, PS(270k)) were purchased from Polymer Source and BP Chemicals, respectively and C_{60} was obtained from MER Corporation (99+% purity) and used as received; solution preparation was described elsewhere[3,4] and vials were wrapped with aluminium foil to block light exposure during sample preparation. Film thicknesses were measured by UV-vis interferometry (Filmetrics, F20-UV). Silicon wafers [100] (ITME Poland) of 380 µm thickness were employed for all experiments except neutron reflectometry, for which 3 mm thick wafers were used. Substrate treatments include: (σ+) as-received substrates, flushed with toluene and dried with nitrogen, (σ–) hydrophobic substrate, rinsed with toluene and dried in ambient conditions for at least 3 days, (σ) piranha treated hydrophobic substrate σ–, cleaned in a bath of 70/30 vol 96% H_2SO_4 (Arga) and 30% H_2O_2 (Fisher Scientific) at 80 °C for 1h, rinsed with excess deionized water and dried with nitrogen. Surface energy calculated by Owens, Wendt, Rabel and Kaelble method based on static contact angle measurements (Easydrop, Kruss GmbH) with (20 µL) polar (deionized water) and non-polar (purified methylene iodide) liquids.

Neutron reflectivity measurements were performed on the D17 reflectometer at Institut Laue-Langevin (ILL), Grenoble, in time-of-flight (TOF) mode using a wavelength range of 2 Å to 20 Å. NR profiles were obtained by measuring two fixed angles of incidence (0.6° and 2.4°). For each sample, the same slit and chopper settings were used yielding format resolution of 3% to 6% across the q_z range plotted in Figure 3. NR data was analyzed using Paratt32 software (version 1.6) from HMI Berlin, with a two-layer model comprising a PS-fullerene 'bulk' layer and a thin (≈1 nm) silicon oxide layer adjacent to the silicon substrate. The model includes six fitting parameters: the thickness (h); the scattering length density (ρ_b) of each layer and the interfacial roughness (σ) between layers. The data was then fitted iteratively using a least-squares fit. Alternative fitting strategies, including fixing surface roughness to the values obtained by AFM or fixing the silicon oxide ρ_b, produced very similar results.

UV and visible light exposure was carried out using, respectively, a 100W UV-A flood light at λ = 365 nm and 0.2 mW/cm^2 (Spectroline SB-100 PA/FB) and an Advanced Illumination source (DL2230) with maximum irradiance of 1.34 mW/cm^2 at 12.5 mm sample-to-light distance, both in ambient conditions for 3–6 h (results obtained under vacuum are reported in Supporting Information). IR-NIR was not explored as C_{60} absorption is very low. Photomasks were designed using AutoCAD and printed with 20k dpi resolution on an acetate sheet (CAD-Art, California); the circuit photomask was obtained from Circuit Graphics Ltd.

Film stability and morphology was observed by reflection optical microscopy (Olympus BX41M, CCD camera AVT Marlin) and AFM (Innova, Bruker). Three-dimensional surface maps were obtained by optical profilometery (Wyko NT9100) in phase shifting interferometry mode. Tetrahydrofuran (THF) was used as a selective solvent for PS in nanocomposite films.

Supporting Information

Supporting Information is available from the Wiley Online Library or from the author.

Acknowledgements

The authors thank EPSRC for funding and Imperial College London for a studentship and graduate award for HCW. George Wang and Koon-Yang Lee (Imperial College London) are acknowledged for their assistance with profilometry and contact angle measurements. The Institut Laue-Langevin, Grenoble, France is gratefully acknowledged for beamtime.

Received: August 23, 2012
Published online: November 9, 2012

[1] K. A. Barnes, A. Karim, J. F. Douglas,A. I. Nakatani, H. Gruell, E. J. Amis, *Macromolecules* **2000**, *33*, 4177.
[2] a) M. A. Holmes, M. E. Mackay, R. K. Giunta, *J. Nanopart. Res.* **2007**, *9*, 753; b) M. A. Yaklin, P. M. Duxbury, M. E. Mackay, *Soft Matter* **2008**, *4*, 2441.
[3] H. C. Wong, J. T. Cabral, *Phys. Rev. Lett.* **2010**, *105*, 038301.
[4] H. C. Wong, J. T. Cabral, *Macromolecules* **2011**, *44*, 4530.
[5] E. S. McGarrity, A. L. Frischknecht, L. J. D Frink, M. E. Mackay, *Phys. Rev. Lett.* **2007**, *99*, 238302.
[6] a) M. E. Mackay, Y. Hong, M. Jeong, S. Hong, T.P. Russell, C.J. Hawker, R. Vestberg, *Langmuir* **2002**, *18*, 1877; b) R. S. Krishnan, M. E. Mackay, C. J. Hawker, B. V. Horn, *Langmuir* **2005**, *21*, 5770.
[7] N. Hosaka, H. Otsuka, M. Hino, A. Takahara, *Langmuir* **2008**, *24*, 5766–5772.
[8] M. E. Mackay, A. Tuteja, P. M. Duxbury, C. J. Hawker, B. Van Horn, Z. Guan, G. Chen, R. S. Krishnan, *Science* **2006**, *311*, 1740.
[9] J. H. Waller, D. G. Bucknall, R. A. Register, H. W. Beckham, J. Leisen, K. Campbell, *Polymer* **2009**, *50*, 4199–4204.
[10] J. D. Gunton, M. San-Miguel, P. S. Sahni, in *Phase Transitions and Critical Phenomena*, (Eds: C. Domb, J. L. Lebowitz), *Vol 8*, pp. 267, Academic, New York **1983**.
[11] G. Reiter, *Phys. Rev. Lett.* **1992**, *68*, 75.
[12] A. Tuteja, M. E. Mackay, S. Narayanan, S. Asokan, M. S. Wong, *Nano. Lett.* **2007**, *7*, 1276.
[13] S. Narayanan, D. R. Lee, R. S. Guico, S. K. Sinha, J. Wang, *Phys. Rev. Lett.* **2005**, *94*, 145504.
[14] P. C. Eklund, P. C. Eklund, A. M. Rao, P. Zhou, Y. Wang, J. M. Holden, *Thin Solid Films* **1995**, *257*, 185.
[15] A. F. Hebard, C. B. Eom, R. M. Fleming, Y. J. Chabal, A. J. Muller, S. H. Glarum, R. C. Haddon, A. M.Mujsce, M. A. Pazkowski, G. P. Kochanski, *Appl. Phys. A* **1993**, *57*, 299.
[16] J. Wang, C. Larsen, T. Wagberg, L. Edman, *Adv. Funct. Mater.* **2011**, *21*, 3723.
[17] F. Cataldo, *Polym. Int.* **1999**, *48*, 143–149.
[18] a) S.-R. Chae, E. M. Hotze, M. R. Wiesner, *Environ. Sci. Technol.* **2009**, *43*, 6208–6213; b) Q. Li, B. Xie, Y. S. Hwang, Y. Xu, *Environ. Sci. Technol.* **2009**, *43*, 3574–3579; c) J. Lee, W. H. Song, S. S. Jang, J. D. Fortner, P. J. J. Alvarez,. W. J. Cooper, J. H. Kim, *Environ. Sci. Technol.* **2010**, *44*(10), 3786–3792; d) Y. S. Hwang, Q. Li, *Environ. Sci. Technol.* **2010**, *44*, 3008–3013.
[19] A. M. Rao, K.-A. Wang, J. M. Holden, Y. Wang, P. Zhou, P. C. Eklund, C. C. Eloi, J. D. Robertson, *J. Mater. Res.* **1993**, *8*, 2277–2281.
[20] A. M. Rao, P. Zhou, K.-A. Wang, G. T. Hager, J. M. Holden, Y. Wang, W.-T. Lee, X.-X. Bi, P. C. Eklund, D. S. Cornett, D. S. Duncan, I. J. Amster, *Science* **1993**, *259*, 955.
[21] G. Z. Li, C. U. Pittman Jr., in *Thin Films And Coatings: New Research* (Eds: B. M. Caruta), Nova Science Publishers, New York **2005**, pp. 1–26.
[22] G. T. Carroll, G. T. Carroll, M. E. Sojka, X. Lei, N. J. Turro, J. T. Koberstein, *Langmuir* **2006**, *22*, 7748–7754.
[23] a) M. Boltau, M. Böltau, S. Walheim, J. Mlynek, G. Krausch, U. Steiner, *Nature* **1998**, *391*, 877; b) A. Karim, J. F. Douglas, B. P. Lee, S. C. Glotzer, J. A. Rogers, R. J. Jackman, E. J. Amis, G. M. Whitesides, *Phys. Rev. E* **1998**, *57*, R6273.
[24] A. M. Higgins, R. A. L Jones, *Nature* **2000**, *404*, 476.

[25] A. Sehgal, V. Ferreiro, J. F. Douglas, E. J. Amis, A. Karim, *Langmuir* **2002**, *18*, 7041.
[26] E. Schaffer, T. Thurn-Albrecht, T. P. Russell, U. Steiner, *Nature* **2000**, *403*, 874.
[27] I. Bita, J. K.W. Yang, Y. S. Jung, C. A. Ross, E. L. Thomas, K. K. Berggren, *Science* **2008**, *321*, 939–943.
[28] M. Jørgensen, K. Norrman, S. A. Gevorgyan, T. Tromholt, B. Andreasen, F. C. Krebs, *Adv. Mater.* **2012**, *24*, 580–612.
[29] J.-C. Wang, J.-C. Wang, C.-Y. Lu, J.-L. Hsu, M.-K. Lee, Y.-R. Hong, T.-P. Peng, S.-F. Hong, H.-F. Meng, *J. Mater. Chem.* **2011**, *21*, 5723.
[30] a) P. Thanikaivelan, N. T. Narayanan, B. K. Pradhan, P. M. Ajayan, *Science* **2002**, *296*, 705. b) J. M. Slocik, A. O. Govorov, R. R. Naik, *Angew. Chem. Int. Ed.* **2008**, *47*, 5335–5339; c) V. Krishna, N. Stevens, B. Koopman, B. Moudgil, *Nat. Nanotechol.* **2010**, *5*, 330–334.